



Cite this: *Digital Discovery*, 2023, 2, 1484

A deep learning model for type II polyketide natural product prediction without sequence alignment†

Jiaquan Huang, ‡^a Qiandi Gao, ‡^a Ying Tang, ^b Yixin Wu, ^a Heqian Zhang *^a and Zhiwei Qin *^a

Natural products are important sources for drug development, and the accurate prediction of their structures assembled by modular proteins is an area of great interest. In this study, we introduce DeepT2, an end-to-end, cost-effective, and accurate machine learning platform to accelerate the identification of type II polyketides (T2PKs), which represent a significant portion of the natural product world. Our algorithm is based on advanced natural language processing models and utilizes the core biosynthetic enzyme, chain length factor (CLF or KS_β), as computing inputs. The process involves sequence embedding, data labeling, classifier development, and novelty detection, which enable precise classification and prediction directly from KS_β without sequence alignments. Combined with metagenomics and metabolomics, we evaluated the ability of DeepT2 and found this model could easily detect and classify KS_β either as a single sequence or a mixture of bacterial genomes, and subsequently identify the corresponding T2PKs in a labeled categorized class or as novel. Our work highlights deep learning as a promising framework for genome mining and therefore provides a meaningful platform for discovering medically important natural products. The DeepT2 is available at GitHub repository: <https://github.com/Qinlab502/deept2>.

Received 8th June 2023
Accepted 29th August 2023

DOI: 10.1039/d3dd00107e
rsc.li/digitaldiscovery

Introduction

Bacterial type II polyketides (T2PKs) are valuable natural products with potent biological activities and comprise a family of structurally related molecules.^{1,2} Illustrative examples include tetracycline, doxorubicin and plicamycin. They are primarily biosynthesized by type II polyketide synthases (T2 PKSs), which catalyze the formation of carbon skeletons in an ordered manner.³ The biosynthetic system is characterized by a minimal set of gene products, of which the most crucial enzymes are the monofunctional heterodimeric β -ketosynthase pair KS_α/KS_β , which catalyze the iterative Claisen condensation using acetyl- and malonyl-CoA as building blocks for chain elongation and determine the chain length and overall topology (Fig. 1A), respectively. In addition, a malonyl transacylase (MT) and an acyl carrier protein (ACP) were taken together with KS_α/KS_β to constitute the minimal T2 PKS systems.⁴ The core skeleton of T2PKs is highly correlated with the KS_α/KS_β protein structure. Hillenmeyer *et al.* observed correlations between KS_β protein

phylogeny and the building blocks of T2PK skeletons,⁵ while Chen *et al.* utilized KS_β as a biomarker to construct a coevolutionary statistical model (phylogenetic tree) to expand the T2PK biosynthetic landscape.⁶ However, the above and other methods^{7–9} frequently rely on multiple sequence alignments, which are time-consuming and do not effectively represent protein structural information.^{10,11}

Several artificial intelligence (AI)-based natural product discovery models have been proposed in recent years due to rapid data accumulation and digital transformation as well as the accelerated development of AI technology.^{12–17} Among these frameworks, deep learning has demonstrated exceptional performance in classification tasks, specifically in the area of distinguishing new and unseen data.^{18–20} For instance, certain deep learning-based tools have demonstrated high efficiency and scalability in predicting natural product classes.^{13,21} However, these tools have limitations when it comes to identifying enzyme sequences that may be involved in the biosynthesis of natural products with novel carbon skeletons. More recently, protein language models (PLMs) based on self-supervised learning have shown remarkable ability to convert individual protein sequences into embeddings that describe the homology between multiple protein sequences and potentially capture physicochemical information not encoded by the existing methods.^{22–24} The application of general PLMs to convert sequences into embeddings, which serve as inputs for deep learning models, effectively overcomes the few-shot

^aCenter for Biological Science and Technology, Advanced Institute of Natural Sciences, Beijing Normal University, Zhuhai, Guangdong, 519087, China. E-mail: z.qin@bnu.edu.cn; zhangheqian@bnu.edu.cn

^bInternational Academic Center of Complex Systems, Advanced Institute of Natural Sciences, Beijing Normal University, Zhuhai, Guangdong, 519087, China

† Electronic supplementary information (ESI) available. See DOI: <https://doi.org/10.1039/d3dd00107e>

‡ These authors contributed equally to this work.



learning challenge for specific biomolecular property predictions.^{25,26} In addition, leveraging the large amount of unlabeled data available through a semi-supervised framework can further improve model performance.^{27,28} Finally, conducting novelty detection on the distribution of sequence-to-chemical feature vectors is a viable approach.²⁹ These advancements inspired us to move forward in understanding T2PKs with PLM, training a robust model with unexplored sequences stored in metagenome data, and eventually finding an effective linker to connect their biosynthetic enzymes and probable chemical structures.

To gain a better approach for the discovery of T2PKs, an end-to-end model named DeepT2 was developed in this study. This model employs multiple classifiers to expedite the translation from protein sequences to the T2PK product class and identify any potential new compounds beyond the established groups. Notably, the model is free of sequence alignment and comprises four main components: (i) sequence embedding: the protein sequences were converted into vector embeddings using a pre-trained PLM called EMS-2;²⁴ (ii) data labeling: the KS_{β} dataset with known corresponding chemical structures was initially split into five classes for labeling based on the total number of

biosynthetic building blocks, which was later reclassified into nine classes through dimension reduction and clustering processes; (iii) classifier development: this was used for both KS_{β} sequences and T2PKs classification; and (iv) novelty detection: Mahalanobis distance-based novelty detection³⁰ was applied to identify any potential new compounds beyond the nine established groups. Remarkably, we leveraged DeepT2 to detect KS_{β} from microbial genomes and successfully identified four T2PKs as categorized in our classifiers. This work paves a promising avenue to further explore the potential of the existing reservoirs of T2PK biosynthetic gene clusters (BGCs) and therefore expand the chemical space of this medically important natural product family.

Results

DeepT2 model architecture

As shown in Fig. 1, the purpose of this study was to develop a methodology for predicting the T2PK class using KS_{β} sequences from bacterial genomes as input. To achieve this, we first used an ensemble of multiple classifiers to determine whether a given protein sequence belongs to KS_{β} , assessed

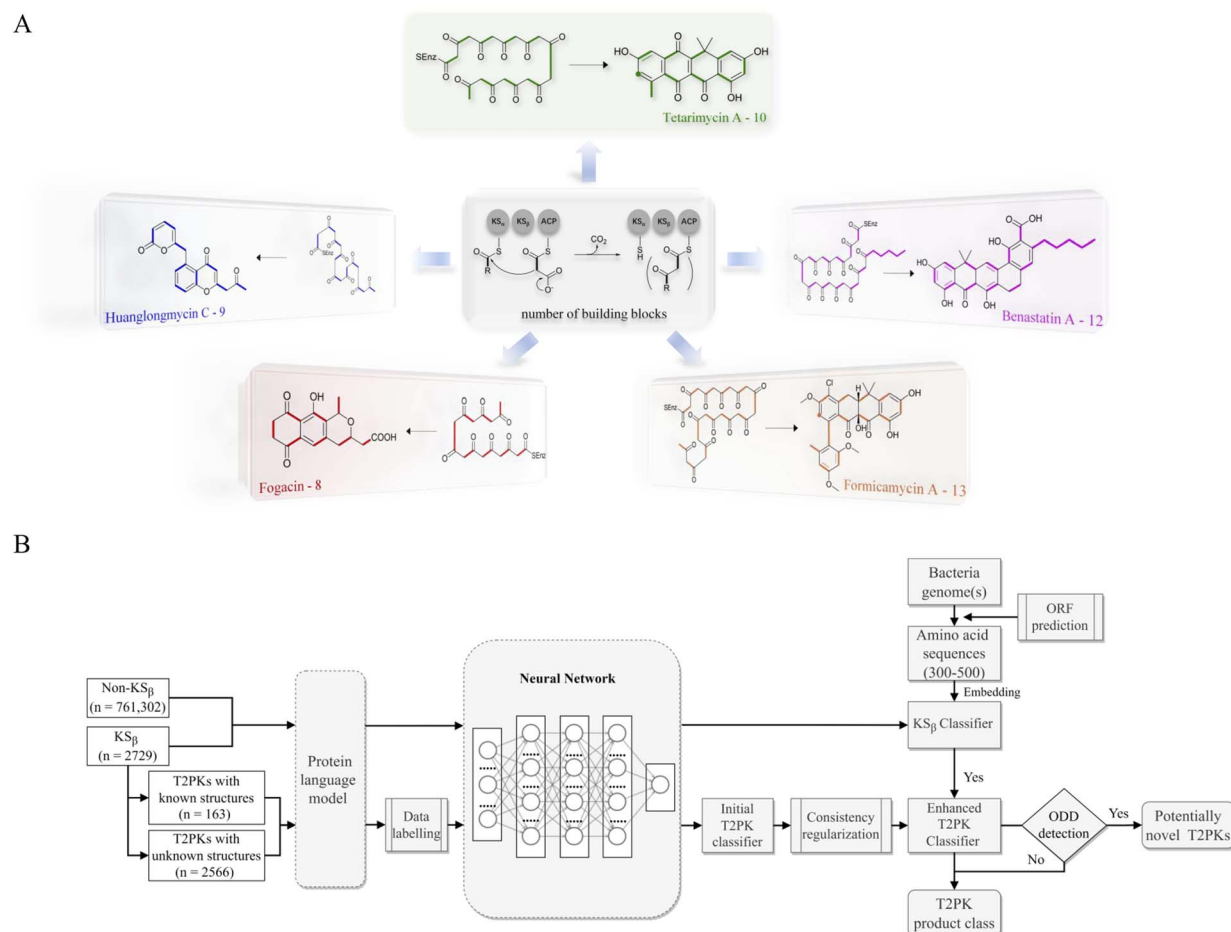


Fig. 1 Illustration of the representative type II polyketides and their biosynthetic intermediates (A) and the overall architecture of DeepT2 developed in this study (B).



Table 1 Pseudocode showing the overall algorithms for DeepT2

Algorithm 1 DeepT2 pseudocode.

Input: Labeled KS_{β} sequences a_i ; Unlabeled KS_{β} sequences a'_i ; Initial label l_i ; non- KS_{β} sequences z_i ; Protein language model PLM .

Def $DeepT2_{KS_{\beta}}(a_i, a'_i, y_i, z_i, PLM)$:

$x_i = PLM(a_i + a'_i, z_i)$
 $y_i \in \{0, 1\}$
 $MLP_{KS_{\beta}} = MLP(FL(y, x))$
Return $MLP_{KS_{\beta}}$

Def $Data_labeling(a_i, y_i, z_i, PLM)$:

$x_i \in PLM(a_i)$
 $y_i \in \{l_i\}$
 $D = UMAP_{\theta}(x_i, y_i)$
 $L = HDBSCAN_{\theta}(D)$
 $\theta = \text{Bayesian optimization (No new label generate = True)}$
Return L

Def $DeepT2_{t2pks}$:

$x_i \in \{a_i\}$
 $x'_i \in \{x | x \notin x_i\}$
 $y_i \in \{L\}$
 $MLP_{t2pks} = MLP(CE(y_i, x_i), MSE(x'_i, noise(x'_i)))$
Return MLP_{t2pks}

Def $ODD_detector$:

Compute confidence score: $M(x) = \max_c - (f(x) - \hat{\mu}_c)^T \hat{\Sigma}^{-1} (f(x) - \hat{\mu}_c)$
Find best layer to detect ODD data: $f(\star)_{best} = SVM(M(KS_{\beta}), M(KS_{\alpha}))$
Train isolation forest model: $IF = \text{isolation forest} \rightarrow s(M(ID)_{f(\star)}, N)$
Return IF

Input: Bacterial genomes g_i

For each genome $g \in 1, \dots, g_i$ **do**

Predict ORF: $AA = \text{prokka} \rightarrow g$
Identify KS_{β} sequences: $q = DeepT2_{KS_{\beta}} \rightarrow AA$
Novel class of T2PK: $r = IF \rightarrow AA$
If $c \notin r$:
 Certain class of T2PK: $c = DeepT2_{t2pks} \rightarrow AA$
end for
Return c, r

whether it fell within or outside the existing labeling product classes, and eventually predicted the product class. General protein language models, including SeqVec, ESM-1b, ESM-2, ProtT5-XL-U50 and ProtBert-BFD, were employed to maximize the use of limited labeled, unlabeled, and non- KS_{β} sequences by converting them into embeddings containing structural representations using the idea of transfer learning. By pretraining on such datasets, PLM can effectively learn general patterns and features that are present in imbalanced data. In this work, the terms of 'labeled KS_{β} ' and 'unlabeled KS_{β} ' indicate whether their corresponding chemical structures are known. KS_{β} and T2PK classifiers were trained by the datasets from the specific protein sequences and chemical structures. To construct a robust T2PK classifier, we applied supervised UMAP (uniform manifold approximation and projection) and HDBSCAN (hierarchical density-based spatial clustering of applications with noise) on the KS_{β} embedding to generate more appropriate class labels and trained the model with unlabeled data on the basis of consistency regularization. Furthermore, the Mahalanobis distance-based algorithm was applied on each feature layer of the T2PK classifier to perform novelty detection and avoid the problem of overconfident. The methodology enabled us not only to classify the known group of T2PKs but also to detect potential novel classes of T2PKs from unknown KS_{β} protein sequences. Detailed results of each process are presented below. The pseudocode for this work has been summarized in Table 1.

Development of the KS_{β} classifier

We obtained a collection of 163 labeled KS_{β} sequences with known corresponding natural product structures (Table S1†) as

well as additional 2566 unlabeled KS_{β} sequences sourced from the RefSeq database, whose associated natural product structures remain unknown (Table S2†). A total of 2729 (163 + 2566) KS_{β} sequences and 761 302 non- KS_{β} sequences were then split into training, validation, and test datasets, as described in the materials and methods section. Prior to constructing the classifier, we employed five general PLMs, including SeqVec, ESM-1b, ESM-2, ProtT5-XL-U50 and ProtBert-BFD respectively, to vectorize each protein sequence for embedding and we observed that the learned representations of ESM-2 and ProtT5-XL-U50 exhibited the best performance compared with the others in distinguishing KS_{β} from non- KS_{β} sequences, as revealed by the results of dimension reduction (Fig. S1†). In this study, we favored ESM-2 because it has the largest parameter size (over 3 billion) and has better performance on the T2PK classifier (see lateral session). Next, we trained the KS_{β} embeddings obtained by the PLMs using four machine learning algorithms, including random forest, XGBoost, support vector machine (SVM) and multilayer perceptron (MLP), and found that MLP and SVM achieved the best results, with an AUROC of 1 and an F1 score of 1 in the classification on the test dataset (Table S3†).

Relabeling 163 T2PKs with constrained optimization approach

Data labeling is crucial for data preprocessing in machine learning, especially for supervised learning.³¹ This is also the most challenging task in this work. Based on prior knowledge, 163 KS_{β} embeddings with known chemical structures were categorized into five groups according to the building block number of their corresponding to T2PK main skeleton, namely, 8, 9, 10, 12 and 13 (Table S1†). However, despite applying ESM-2 to the 163 KS_{β} sequences, imprecise representation of the distribution pattern of the 5 label embeddings was observed (Fig. S2A†), probably due to the inadequate fittings between some of the class labels and the protein embeddings. To address this issue, a constrained optimization approach was developed to correct the improper class labels for each sample and further separate their local features from global features to generate new class labels (Fig. 2B). Specifically, we employed supervised UMAP and HDBSCAN as regularization techniques to constrain the latent distribution of KS_{β} embeddings and automatically tune UMAP and HDBSCAN hyperparameters using a labeling cost function to assign more appropriate class labels to the embeddings. Of note, the supervised UMAP opted for this study incorporates compound skeleton labels into the optimization process to ensure that the resulting reduced-dimensional space consistently captures the features of the compound skeleton. It is worth noting that unsupervised UMAP, in contrast to its supervised counterpart, lacks access to labeled data during the optimization process. Consequently, this absence of label supervision poses a challenge in ensuring the consistent representation of compound skeleton features within the reduced-dimensional space.

As illustrated in Fig. 2A, the restructuring process of KS_{β} embeddings initially reset the counts of predefined labels to 3,



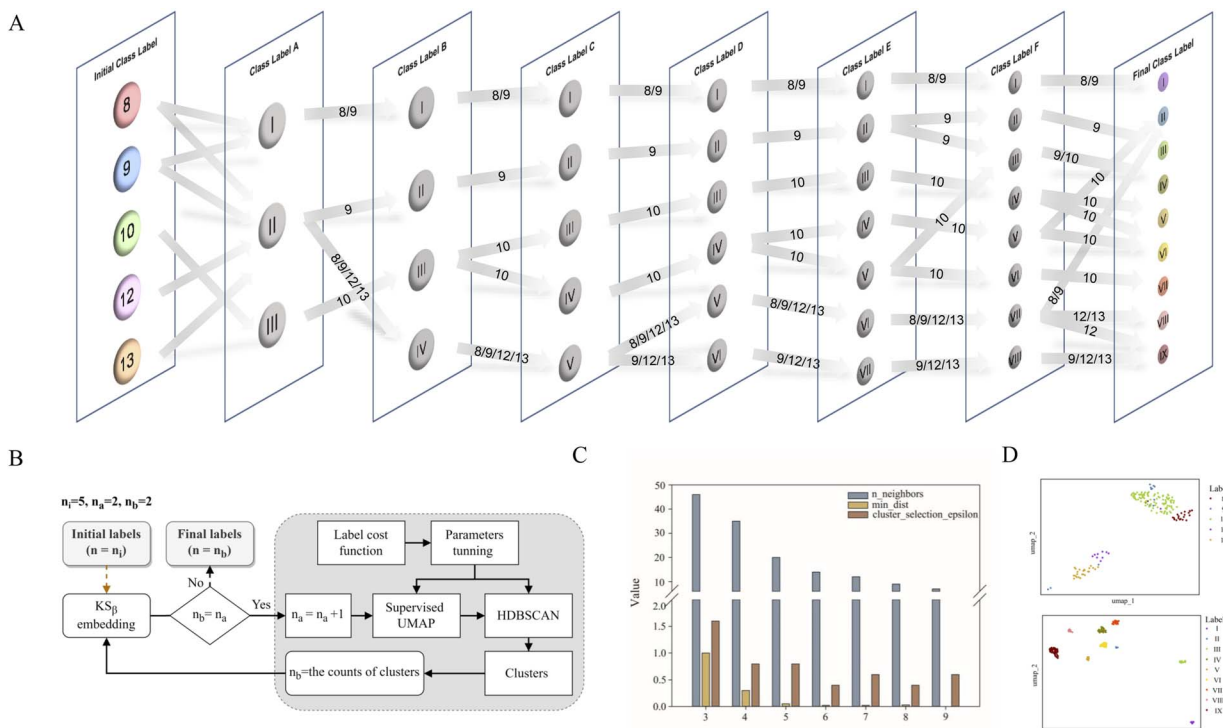


Fig. 2 The flowchart showing the process of KS_{β} labeling (A) and the applications of supervised UMAP and HDBSCAN algorithms (B), the parameter optimizations during the process of A and B (C), and the supervised UMAP comparison of T2PK class labeling generated by five manually annotated class labels (up, D) and nine refined class labels (bottom, D).

followed by the automatic adjustment of the $n_{\text{neighbors}}$ and min_dist parameters to refine the space and improve its alignment with these 3 class labels. HDBSCAN was then applied to cluster the similar data points and assign new class labels to them. Certain previously assigned KS_{β} sequences were bifurcated and merged into a new label. For example, in class label A column, label I is from partial initial label 8 and 9; label II is from partial initial label 8 and 9, and entire initial 12 and 13; and label III is from entire initial label 10 (Fig. 2A, Table S4†). Upon increasing the number of predefined labels, the approach tuned the $n_{\text{neighbors}}$ and min_dist parameters to decrease their values, which allowed HDBSCAN to recognize and assign new labels to smaller and more localized features in the data space (Fig. 2C and S3†). This iterative process continued until the number of class labels assigned to the 163 KS_{β} embeddings reached 9, after which no more labels could be generated or some data points were identified as noise. To evaluate the distribution patterns of the 9 autogenerated labels, the supervised UMAP technique was employed again, revealing that these labels could represent the T2PK biosynthetic logics more accurately in the real world (Fig. 2D).

Development of the T2PK classifier

As described in the previous session, four machine learning algorithms (random forest, XGBoost, SVM, and MLP with grid search hyperparameter tuning) were employed to train the initial T2PK classifiers on KS_{β} embeddings. The classifiers were

trained on two distinct sets of class labels: one comprising five manually annotated class labels and another consisting of nine refined class labels (Fig. 2D). Due to the imbalanced nature of our dataset, the F1 score and confusion matrix were employed to assess and compare the performance of the classifiers trained on these two different sets of class labels. As outlined in Table 2, the MLP classifier yielded an F1 score of 0.89 on the test set when utilizing the nine refined class labels, whereas the F1 scores of the random forest, XGBoost, and SVM classifiers were 0.77, 0.73, and 0.92, respectively. Notably, the classifiers trained on the five manually annotated class labels exhibited inferior performance compared with those trained on the nine refined class labels.

To leverage the 2566 unlabeled KS_{β} embeddings, a consistency regularization-based semi-supervised learning framework was adopted to train an enhanced MLP classifier based on the initial MLP classifier with two distinct sets of class labels. The enhanced MLP classifier was trained on both labeled and unlabeled data. In this process, the cross-entropy loss function was applied to the disturbed labeled data *via* Gaussian noise, while the mean-square error loss function was applied to both disturbed labeled and unlabeled data (Fig. 3A). This approach promoted the model to produce consistent predictions over time and resulted in a smoothed decision boundary, thereby enhancing the model's generalization performance on unseen data and alleviating overfitting. A clear disturbance in the initial classifier at the beginning is shown in Fig. 3B. Overall, the performance evaluation demonstrated that the enhanced MLP

Table 2 Performance metrics of initial and enhanced T2PK classifier with two types of class label trained by random forest, XGBoost, SVM, MLP. TPR: true positive rate; FPR: false positive rate

Classifier	Class number	TPR%	FPR%	Accuracy	Precision	Recall	F1-score
Initial classifier							
Random forest	5 classes	55.00	8.88	0.76	0.49	0.55	0.51
	9 classes	76.11	2.81	0.79	0.80	0.76	0.77
XGBoost	5 classes	57.67	8.88	0.76	0.68	0.58	0.59
	9 classes	76.11	2.73	0.79	0.75	0.76	0.73
SVM	5 classes	62.67	7.02	0.79	0.80	0.63	0.66
	9 classes	96.76	0.68	0.94	0.91	0.97	0.92
MLP	5 classes	67.56	5.25	0.79	0.67	0.68	0.67
	9 classes	93.15	1.51	0.88	0.87	0.93	0.89
Enhanced classifier							
MLP	5 classes	66.67	6.38	0.82	0.91	0.67	0.70
	9 classes	97.78	0.43	0.97	0.99	0.98	0.98

classifier trained with nine refined class labels attained an F1 score of 0.98 on the test set, an increase of 0.09 compared with the initial one, indicating state-of-the-art performance.

Out-of-distribution detection (ODD) for new T2PKs

Softmax-based classifiers have been criticized for generating overconfident posterior distributions when presented with ODD data.³² In this study, ODD data refer to KS_{β} sequences that do not belong to any of the nine refined classes as described above. To overcome this limitation, we incorporated Mahalanobis distance-based scores (MDS) and anomaly detection techniques inspired by the generalized ODD framework:²⁹

$$\begin{cases} M(x) = \max_c - (f(x) - \hat{\mu})^T \hat{\Sigma}^{-1} (f(x) - \hat{\mu}_c) \\ f(\bullet)_{\text{best}} = M(KS_{\alpha}) \rightarrow SVM \odot M(KS_{\beta}) \end{cases}$$

where the Mahalanobis distance-based scores, denoted as $M(x)$, is determined by evaluating the empirical class mean $\hat{\mu}$ and covariance $\hat{\Sigma}$ of the training samples; \odot represents the utilization of the one-class SVM to detect $M(KS_{\beta})$ for each feature layer.

Of note, we designated 163 KS_{α} sequences as ODD data and 163 KS_{β} sequences as in-distribution (ID) data and extracted feature vectors from the neural network consisting of input, hidden ($n = 3$), and output layers of the MLP classifier to

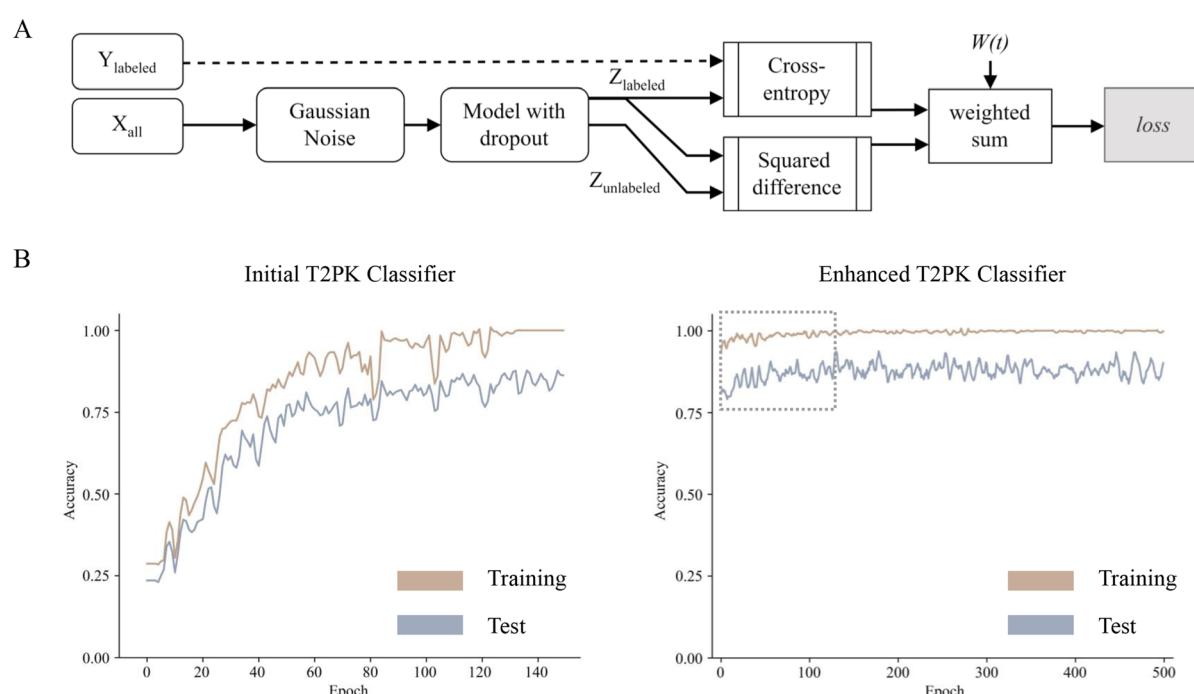


Fig. 3 The flowchart showing the development of T2PK classifier using consistency regularization-based semi-supervised learning approach (A); plots showing the accuracies of prediction for the initial (left, B) and enhanced (right, B) T2PK classifiers.



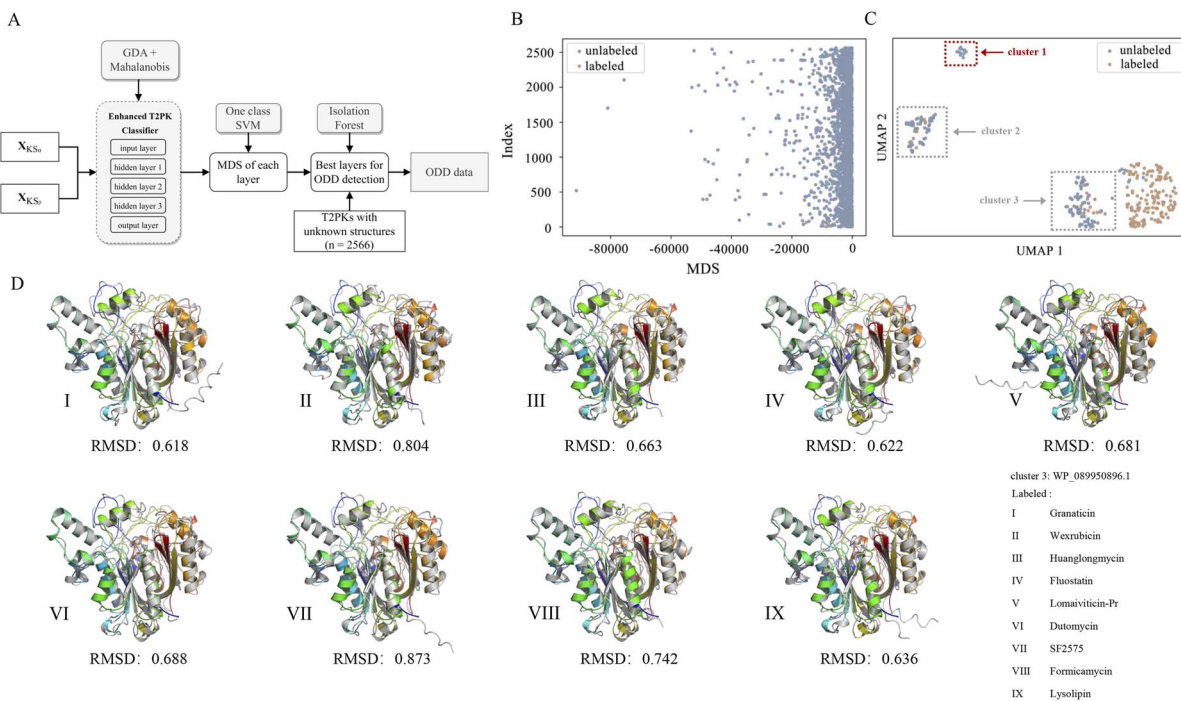


Fig. 4 The flowchart showing the process for detecting novel T2PKs (A), the MDS distribution of 163 labeled KS_β and 2566 unlabeled KS_β within hidden layer 1 (B), ODD clusters (C), and the representative *in silico* predictions of the protein structures generated by ESMFold (D), grey structure indicates the labeled KS_β for the biosynthesis of known T2PK, while colour structures indicate unlabeled KS_β from cluster 1 in C, respectively.

compute the MDS for both ID and ODD data (Fig. 4A). We evaluated the classification performance of each layer using a one-class SVM on the ID and ODD datasets and found that the hidden layer 1 exhibited superior performance in detecting ODD data (Fig. S4†). Further, we present the MDS distribution of 163 labeled KS_β sequences (ID data) and 2566 non-labeled KS_β sequences within hidden layer 1. In Fig. 4B, some data points within the unlabeled KS_β sequences conspicuously diverge from the cluster of the ID data.

Next, we utilized the MDS data generated from hidden layer 1 to train an isolation forest model. This model was then employed to detect ODD data within a larger dataset comprising unlabeled sequences:

$$\left\{ \begin{array}{l} s(x_i, N) = 2^{\frac{-E(h(x_i))}{c(N)}} \\ \text{ODD} = \text{IF} \odot s(M(\text{ID})_{f(\bullet)}, N) \end{array} \right.$$

where $s(x_i, N)$ represents anomaly score; and the computed anomaly score from $M(\text{ID})_{f(\bullet)}$ is fitted using the IF algorithm to detect ODD data points in unknown input data. In this manner, a total of 164 sequences were identified as ODD data points from a pool of 2566 unlabeled sequences.

To facilitate a more comprehensive visualization of the distribution of abnormal datasets, we combined the labeled and abnormal datasets and conducted UMAP dimension reduction. Through this process, we were able to identify three clusters, labeled as ODD clusters, which encompassed a total of 164 abnormal data points. On one hand, certain data points from ODD clusters 2 and 3 were found to overlap with the

labeled dataset, as indicated by the grey dotted box in Fig. 4C. This occurrence does not imply inaccuracies in the detection process; rather, it suggests that the KS_β from these two clusters share some similarities in their embeddings with the labeled sequences. This observation further suggests that the corresponding chemical structures of these data points may possess common characteristics with the structurally known T2PKs. On the other hand, we noticed that ODD cluster 1, comprising 13 sequences, was completely separated from the labeled dataset and situated at a considerable distance, as shown in Fig. 4C. Based on our hypothesis, the KS_β proteins within this ODD cluster may exhibit novel catalytic domains that differ from the previously labeled KS_β proteins. It is plausible to assume that these novel domains are potentially involved in the biosynthesis of previously undiscovered T2PKs.

To test this hypothesis, we employed ESMFold to conduct *in silico* predictions of protein structures for all data points within ODD cluster 1. We then calculated the root mean square deviation (RMSD) between the predicted structures of the 13 unlabeled KS_β proteins and the 163 labeled KS_β proteins. The average RMSD value between the protein structures in ODD cluster 1 and those in classes IV, V, VI, and VII was found to be 0.58 Å (Fig. S5 and Table S5†). Table S6† provides the calculated RMSD values between ODD cluster 1 and classes IV–VII, and based on these values, a threshold of 0.4 can be set to distinguish between intra-class and inter-class structures. This indicates that, for the exploration of novel T2PKs, particular attention should be given to KS_β proteins with an RMSD value exceeding 0.4 between the ODD cluster and other classes, as depicted in Fig. 4D.

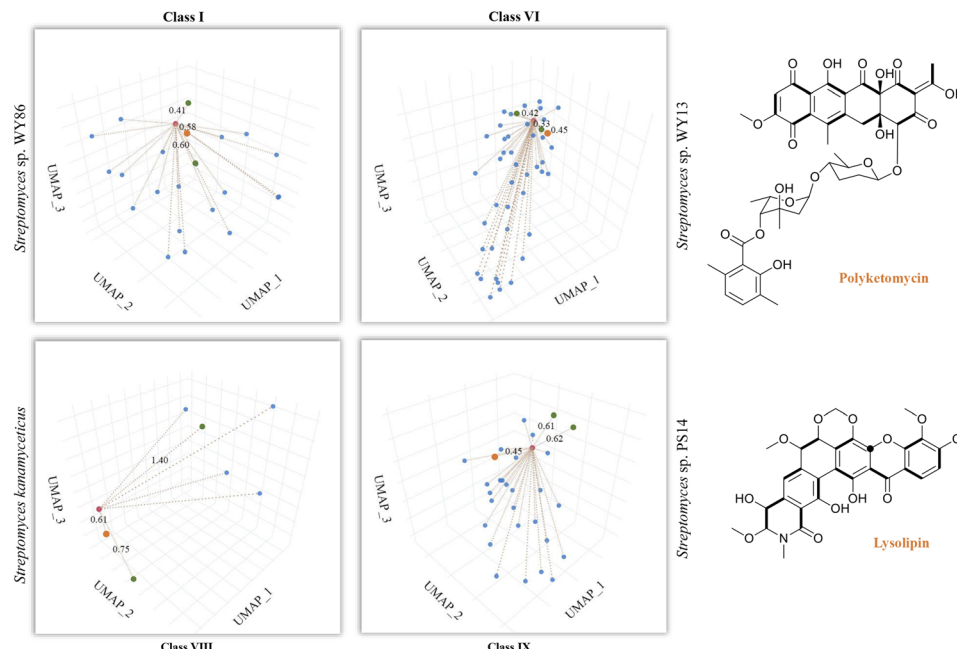


Fig. 5 T2PK prediction from bacterial genomes. DeepT2 was performed and the identified compounds alnumycin A, polyketomycin, and lysolipin were subsequently confirmed via high-resolution mass spectra (Fig. S6†). Euclidean distances for each predicted candidate with top 3 similar T2PKs were annotated beside the dash lines (red, T2PKs to be detected; orange, the most similar T2PKs experimentally confirmed; green, other similar T2PKs that have close KS_{β} structures but different natural products). Further information can be found in Table S7.† The ground-truth T2PK of bacteria is denoted by the orange point in each figure. Bold bonds in each chemical structure indicate the building block units incorporated into the polyketide backbone, while the black dot indicates a single carbon from the build block unit in which the adjacent carbon from the same build block is lost during the polyketide biosynthesis via decarboxylation.

Predicting T2PKs from bacterial genomes

So far, our findings have demonstrated the effectiveness of DeepT2 in accelerating the identification of T2PKs. We were therefore motivated to explore the advantages of this model in uncovering the potential of any T2PKs produced by actinomycetes isolated or stored in our laboratory. As such, we sequenced 5 *Streptomyces* strains and confirmed their genomic independence through average nucleotide identity comparison. Following that, we employed DeepT2, DeepBGC, and antiSMASH³³ to predict the T2PK produced from these 5 strains. Our findings demonstrate that DeepT2 surpasses DeepBGC and antiSMASH in terms of T2PK prediction, as the latter two tools primarily focus on identifying the BGCs rather than specifically targeting T2PKSs. In addition, we investigated the ability of these tools to handle metagenomic sequences by combining the 5 genomes and subjecting them to the aforementioned tools. The results revealed that only DeepT2 is capable of handling metagenomic input, yielding identical outputs to those obtained from individual genome inputs. On the other hand, neither the web server nor the local version of antiSMASH allows for direct submission of metagenomic sequences. Furthermore, we evaluated the performance of these tools on single-gene input by extracting candidate KS_{β} sequences from the 5 genomes and submitting them as individual sequences to the mentioned tools. It was observed that only DeepT2 supported single-gene input and produced accurate predictions (Table S7†).

In this way, we selected three top closest ID sample as predicted T2PK for the unknown KS_{β} input. As an overall result, 10 KS_{β} protein sequences were detected from 5 *Streptomyces* genome that fell into four classes (Table S7†), and the corresponding T2PKs were closest to alnumycin, granaticin and frenolicin in class I,^{34–36} polyketomycin, dutomycin and LL-D49194 in class VI,^{37–39} fasamycin, formicamycin and Sch in class VIII,^{40–42} and lysolipin, BE-24566B and anthrabenzoxocinone in class IX,^{43–45} respectively (Fig. 5 and Table S7†). To confirm this prediction, the strains were then inoculated and their metabolites were analyzed by liquid chromatography high-resolution mass spectrometry. As the result, alnumycin from WY86, polyketomycin from WY13 and lysolipin from PS14 were observed (Fig. 5 and S6†), whereas fasamycin from *S. kanamyceticus* was not detected under laboratory conditions as described in a recent study.⁴⁶

Discussion

T2 polyketide synthase is a family of single heterodimeric ketosynthases that iteratively catalyzes the elongation of the polyketide chain structure, leading to our inability to precisely predict T2PK structures. As introduced previously, despite the multiple sequence alignment approaches based on KS_{β} ,^{5,6} incorporation of new sequences into the evolutionary model may alter the structure of the original phylogenetic tree and therefore compromise the accuracy of the predictions. To address this issue, we propose DeepT2, an end-to-end deep



learning strategy, to directly identify T2PKs from bacterial genomes. Leveraging the concept of natural language processing, our approach embeds KS_{β} as feature vectors, enabling the representation of protein structural information. We employ semi-supervised learning to link KS_{β} embedding vectors with compound labels, facilitating the rapid identification of known and novel T2PKs. Importantly, in contrast to other BGC prediction tools, such as DeepBGC²¹ and antiSMASH, which require complete T2PK BGC sequences, our DeepT2 model can accurately predict T2PK categories using only KS_{β} sequences. Furthermore, our novelty detection framework embedded in DeepT2 has promising potential for identifying new KS_{β} . However, a question that may arise is that considering the limited biological data volume, is it still possible to use it to develop advanced algorithms even without big data? This is because in the biological research field, classic machine learning and currently popular deep learning are both hampered by poor accuracy or overfitting caused by the smaller training dataset. Indeed, during model development, we had debated whether the proof of concept should be data-centered or training-centered. Fortunately, the ensemble method using a small data volume based on pretraining and semi-supervised learning seems to be a promising solution, at least for this work. In addition, as with other machine learning algorithms, DeepT2 is expected to improve as more KS_{β} sequences are discovered in microbial genomes over time.

The task of few-shot supervised learning requires an approach that transcends traditional supervised neural networks.⁴⁷ In this context, our work adopts the concept of transfer learning, where ESM-2 is utilized to explore the connection between KS_{β} embeddings and T2PK structures. While the dimension reduction results indeed indicate that the embedding vectors obtained by ESM-2 closely fit with the compound class labels, it is important to note that certain embeddings still necessitate further labeling refinement and correction. Consequently, we performed label reconstruction using supervised UMAP instead of unsupervised UMAP to ensure that the resulting reduced-dimensional space consistently captures the features of the compound skeleton. This approach differs from traditional unsupervised learning for clustering,⁴⁸ as it strives to strike a balance between the sequence embeddings and the compound class labels to improve the model's accuracy. For example, T2PK AQ-256-8 consists of 8 building blocks, but its KS_{β} is confirmed as ancestral nonoxidative, which differs from other KS_{β} s that involve the biosynthesis of T2PKs with 8 building blocks.⁶ Clearly, the state-of-the-art performance of the model trained with 9 refined class labels suggests that the classification effect is unsatisfactory when simply using five biosynthetic building blocks as labels. This finding suggests that KS_{β} not only affects the counts of building blocks but also determines a rough topology prior to cyclization or aromatization. To the best of our knowledge, this is the first algorithm for T2PK classification and prediction in such a manner, which, as an alternative to sophisticated protein sequence alignment, might showcase a paradigm shift in genome-mining approaches for natural product discovery.

As shown above, we improved the generalization ability of the softmax-based T2PK classifier by employing a consistency-regularization-based semi-supervised learning framework that utilized 2566 KS_{β} whose corresponding natural product structures currently remain unknown. However, such models may demonstrate overconfidence in discerning novel KS_{β} sequences in the real world.³² To address this concern, an ODD framework based on the Mahalanobis distance was implemented for multiclass novelty detection.⁴⁹ Notably, certain samples (from 2566 KS_{β} sequences) are proximal to the labeled data (from 163 KS_{β} sequences) because such labeled T2PKs with entirely novel carbon skeletons have only been discovered in recent years, such as formicamycin⁴⁰ and dendrubicin.⁵⁰ Therefore, to avoid false positives in novelty detection, we selected only 13 potential new class samples that are distant from the labeled samples for demonstration. Greater details regarding the enzymatic information and chemical structures for these T2PKs will be studied in future work.

This study demonstrates the capacity of DeepT2 to predict T2PKs from single or mixed genomic datasets. However, some limitations must be acknowledged. While the training data included bacterial genomes from different phyla, certain biases may hinder the model's ability to detect novel T2PKs in poorly characterized bacterial sources within complex microbiomes. Although the model was validated using *Streptomyces* genomes as a showcase in this study, it is essential to expand the collection of bacterial genomes to enhance the overall performance of the model. Additionally, the current version of DeepT2 is capable of predicting T2PKs from single genes as input, but it requires complete sequences of at least 300 amino acids (the average length of KS_{β} is around 400 amino acid). For predicting other tailoring modifications, such as methylation or halogenation, supplementing DeepT2 with antiSMASH or DeepBGC is recommended. Nonetheless, despite these limitations, the DeepT2 model outperforms other methods and represents a valuable algorithm for KS_{β} identification and T2PK discovery. This study also inspires future research to identify which catalytic domains in KS_{β} contribute to chemical differences through PLM and thus provides more insights into the KS_{β} evolution and T2PK biosynthetic mechanisms, and this is currently ongoing in our laboratory. Moreover, as the application of language models in prompt tuning for zero-shot prediction, as well as the generative models such as autoregressive neural networks is gradually emerging,⁵¹⁻⁵³ we are now prompted to explore such models for KS_{β} studies. We therefore anticipate that this work will aid in the application of genome mining approaches to discover new KS_{β} and novel T2PKs and have important clinical implications for transforming microbiome data into therapeutic interventions.

Data availability

The authors declare that the data, materials and code supporting the findings reported in this study are available from the authors upon reasonable request. The DeepT2 is available at GitHub repository <https://github.com/Qinlab502/deept2>.



Author contributions

Zhiwei Qin and Heqian Zhang designed and supervised the research, Jiaquan Huang and Qiandi Gao performed the bio-informatic and computing analysis, Yaxin Wu performed the microbial fermentation and chemical analysis, Ying Tang participated the algorithm development. All authors analysed and discussed the data. Zhiwei Qin, Heqian Zhang and Jiaquan Huang wrote the manuscript and all authors commented.

Conflicts of interest

There are no conflicts to declare.

Acknowledgements

This work was supported by the National Natural Science Foundation of China (32170079, 32200035 and 12105014), the Natural Science Foundation of Guangdong (2021A1515012026), Guangdong Talent Scheme (2021QN020100), Beijing Normal University *via* the Youth Talent Strategic Program Project (310432104), as well as Guangdong Innovation Research Team for Plant-Microbe Interaction. We also thank the Interdisciplinary Intelligence Super Computer Center, Beijing Normal University at Zhuhai, for High Performance Computing for access to computational resources.

Notes and references

- 1 S.-C. Tsai, *Annu. Rev. Biochem.*, 2018, **87**, 503–531.
- 2 C. Hertweck, A. Luzhetskyy, Y. Rebets and A. Bechthold, *Nat. Prod. Rep.*, 2007, **24**, 162–190.
- 3 C. Hertweck, *Angew. Chem., Int. Ed.*, 2009, **48**, 4688–4716.
- 4 A. Bräuer, Q. Zhou, G. L. Grammbitter, M. Schmalhofer, M. Rühl, V. R. Kaila, H. B. Bode and M. Groll, *Nat. Chem.*, 2020, **12**, 755–763.
- 5 M. E. Hillenmeyer, G. A. Vandova, E. E. Berlew and L. K. Charkoudian, *Proc. Natl. Acad. Sci. U. S. A.*, 2015, **112**, 13952–13957.
- 6 S. Chen, C. Zhang and L. Zhang, *Angew. Chem., Int. Ed.*, 2022, **61**, e202202286.
- 7 C. P. Ridley, H. Y. Lee and C. Khosla, *Proc. Natl. Acad. Sci. U. S. A.*, 2008, **105**, 4595–4600.
- 8 J. Kim and G.-S. Yi, *BMC Microbiol.*, 2012, **12**, 1–12.
- 9 R. Villebro, S. Shaw, K. Blin and T. Weber, *J. Ind. Microbiol. Biotechnol.*, 2019, **46**, 469–475.
- 10 E. C. Alley, G. Khimulya, S. Biswas, M. AlQuraishi and G. M. Church, *Nat. Methods*, 2019, **16**, 1315–1322.
- 11 A. Elnaggar, M. Heinzinger, C. Dallago and B. Rost, *bioRxiv*, 2019, DOI: [10.1101/864405](https://doi.org/10.1101/864405).
- 12 N. J. Merwin, W. K. Mousa, C. A. Dejong, M. A. Skinnider, M. J. Cannon, H. X. Li, K. Dial, M. Gunabalasingam, C. Johnston and N. A. Magarvey, *Proc. Natl. Acad. Sci. U. S. A.*, 2020, **117**, 371–380.
- 13 C. Rios-Martinez, N. Bhattacharya, A. P. Amini, L. Crawford and K. K. Yang, *PLoS Comput. Biol.*, 2023, **19**, e1011162.
- 14 Y. Ma, Z. Guo, B. Xia, Y. Zhang, X. Liu, Y. Yu, N. Tang, X. Tong, M. Wang and X. Ye, *Nat. Biotechnol.*, 2022, **40**, 921–931.
- 15 V. J. Sahayashela, M. B. Lankadasari, V. M. Dan, S. G. Dastager, G. N. Pandian and H. Sugiyama, *Nat. Prod. Rep.*, 2022, **39**, 2215–2230.
- 16 F. I. Saldívar-González, V. D. Aldas-Bulos, J. L. Medina-Franco and F. Plisson, *Chem. Sci.*, 2022, **13**, 1526–1546.
- 17 D. W. P. Tay, N. Z. X. Yeo, K. Adaikappan, Y. H. Lim and S. J. Ang, *Sci. Data*, 2023, **10**, 296.
- 18 Y. Tang and A. Hoffmann, *Rep. Prog. Phys.*, 2022, **85**, 086602.
- 19 L. Yann, B. Yoshua and H. Geoffrey, *Nature*, 2015, **521**, 436–444.
- 20 H. W. Kim, M. Wang, C. A. Leber, L. F. Nothias, R. Reher, K. B. Kang, J. J. J. van der Hooft, P. C. Dorrestein, W. H. Gerwick and G. W. Cottrell, *J. Nat. Prod.*, 2021, **84**, 2795–2807.
- 21 G. D. Hannigan, D. Prihoda, A. Palicka, J. Soukup, O. Klempir, L. Rampula, J. Durcak, M. Wurst, J. Kotowski, D. Chang, R. R. Wang, G. Piizzi, G. Temesi, D. J. Hazuda, C. H. Woelk and D. A. Bitton, *Nucleic Acids Res.*, 2019, **47**, e110.
- 22 A. Rives, J. Meier, T. Sercu, S. Goyal, Z. Lin, J. Liu, D. Guo, M. Ott, C. L. Zitnick and J. Ma, *Proc. Natl. Acad. Sci. U. S. A.*, 2021, **118**, e2016239118.
- 23 S. Unsal, H. Atas, M. Albayrak, K. Turhan, A. C. Acar and T. Doğan, *Nat. Mach. Intell.*, 2022, **4**, 227–245.
- 24 Z. Lin, H. Akin, R. Rao, B. Hie, Z. Zhu, W. Lu, N. Smetanin, R. Verkuil, O. Kabeli and Y. Shmueli, *Science*, 2023, **379**, 1123–1130.
- 25 F. Teufel, J. J. Almagro Armenteros, A. R. Johansen, M. H. Gíslason, S. I. Pihl, K. D. Tsirigos, O. Winther, S. Brunak, G. von Heijne and H. Nielsen, *Nat. Biotechnol.*, 2022, **40**, 1023–1025.
- 26 M. H. Hoie, E. N. Kiehl, B. Petersen, M. Nielsen, O. Winther, H. Nielsen, J. Hallgren and P. Marcatili, *Nucleic Acids Res.*, 2022, **50**, W510–W515.
- 27 H. Song, M. Kim, D. Park, Y. Shin and J.-G. Lee, *IEEE Trans. Neural Netw. Learn. Syst.*, 2022, DOI: [10.1109/TNNLS.2022.3152527](https://doi.org/10.1109/TNNLS.2022.3152527).
- 28 Y. Ouali, C. Hudelot and M. Tami, *arXiv*, 2020, preprint arXiv:2006.05278, DOI: [10.48550/arXiv.2006.05278](https://doi.org/10.48550/arXiv.2006.05278).
- 29 J. Yang, K. Zhou, Y. Li and Z. Liu, *arXiv*, 2021, preprint arXiv:2110.11334, DOI: [10.48550/arXiv.2110.11334](https://doi.org/10.48550/arXiv.2110.11334).
- 30 K. Lee, K. Lee, H. Lee and J. Shin, *arXiv*, 2018, preprint, arXiv:1807.03888, DOI: [10.48550/arXiv.1807.03888](https://doi.org/10.48550/arXiv.1807.03888).
- 31 L. Zhou, S. Pan, J. Wang and A. V. Vasilakos, *Neurocomputing*, 2017, **237**, 350–361.
- 32 A. Nguyen, J. Yosinski and J. Clune, *arXiv*, 2015, preprint, arXiv:1412.1897, DOI: [10.48550/arXiv.1412.1897](https://doi.org/10.48550/arXiv.1412.1897).
- 33 B. Kai, S. Simon, K. Alexander M, C.-P. Zach, V. W. Gilles P, M. Marnix H and W. Tilmann, *Nucleic Acids Res.*, 2021, **49**, W29–W35.
- 34 T. Oja, L. Niiranen, T. Sandalova, K. D. Klika, J. Niemi, P. Mantsala, G. Schneider and M. Metsa-Ketela, *Proc. Natl. Acad. Sci. U. S. A.*, 2013, **110**, 1291–1296.



35 K. Ichinose, D. J. Bedford, D. Tornus, A. Bechthold, M. J. Bibb, W. P. Revill, H. G. Floss and D. A. Hopwood, *Chem. Biol.*, 1998, **5**, 647–659.

36 C. Han, Z. Yu, Y. Zhang, Z. Wang, J. Zhao, S.-X. Huang, Z. Ma, Z. Wen, C. Liu and W. Xiang, *J. Agric. Food Chem.*, 2021, **69**, 2108–2117.

37 M. Daum, I. Peintner, A. Linnenbrink, A. Frerich, M. Weber, T. Paululat and A. Bechthold, *ChemBioChem*, 2009, **10**, 1073–1083.

38 L.-J. Xuan, S.-H. Xu, H.-L. Zhang, Y.-M. Xu and M.-Q. Chen, *J. Antibiot.*, 1992, **45**, 1974–1976.

39 W. J. Underberg, G. A. Hofman, S. C. Lubbers, O. Bekers, W. W. Ten Bokkel Huinink and J. H. Beijnen, *J. Pharm. Biomed. Anal.*, 1989, **7**, 1791–1797.

40 Z. Qin, J. T. Munnoch, R. Devine, N. A. Holmes, R. F. Seipke, K. A. Wilkinson, B. Wilkinson and M. I. Hutchings, *Chem. Sci.*, 2017, **8**, 3218–3227.

41 Z. Qin, R. Devine, T. J. Booth, E. H. Farrar, M. N. Grayson, M. I. Hutchings and B. Wilkinson, *Chem. Sci.*, 2020, **11**, 8125–8131.

42 G. Blanco, P. Brianb, A. Pereda, C. Mendez, J. Salas and K. F. Chater, *Gene*, 1993, **130**, 107–116.

43 P. Lopez, A. Hornung, K. Welzel, C. Unsin, W. Wohlleben, T. Weber and S. Pelzer, *Gene*, 2010, **461**, 5–14.

44 K. Kojiri, S. Nakajima, A. Fuse, H. Suzuki and H. Suda, *J. Antibiot.*, 1995, **48**, 1506–1508.

45 K. B. Herath, H. Jayasuriya, Z. Guan, M. Schulman, C. Ruby, N. Sharma, K. MacNaul, J. G. Menke, S. Kodali and A. Galgoci, *J. Nat. Prod.*, 2005, **68**, 1437–1440.

46 K. Jiang, X. Yan, Z. Deng, C. Lei and X. Qu, *J. Nat. Prod.*, 2022, **85**, 943–950.

47 W. Yaqing, Y. Quanming, K. James T and N. Lionel M, *ACM Comput. Surv.*, 2020, **53**, 1–34.

48 M. S. Asyaky and R. Mandala, 2021.

49 K. Lee, K. Lee, H. Lee and J. Shin, *Adv. Neural Inf. Process Sys.*, 2018, **31**.

50 K. Ishida, G. Shabuer, S. Schieferdecker, S. J. Pidot, T. P. Stinear, U. Knuepfer, M. Cyrulies and C. Hertweck, *Chem. - Eur. J.*, 2020, **26**, 13147–13151.

51 P. Liu, W. Yuan, J. Fu, Z. Jiang, H. Hayashi and G. Neubig, *ACM Comput. Surv.*, 2023, **55**, 1–35.

52 Y. Tang, J. Weng and P. Zhang, *Nat. Mach. Intell.*, 2023, 1–10, DOI: [10.1038/s42256-023-00632-6](https://doi.org/10.1038/s42256-023-00632-6).

53 J. Trinquier, G. Uguzzoni, A. Pagnani, F. Zamponi and M. Weigt, *Nat. Commun.*, 2021, **12**, 5800.

